

Rationally Designed Nucleoside Antibiotics That Inhibit Siderophore Biosynthesis of *Mycobacterium tuberculosis*

Ravindranadh V. Somu,[†] Helena Boshoff,[‡] Chunhua Qiao,[†] Eric M. Bennett,[†] Clifton E. Barry III,[‡] and Courtney C. Aldrich^{†,*}

Center for Drug Design, Academic Health Center, University of Minnesota, Minneapolis, Minnesota 55455, and Tuberculosis Research Section, National Institute of Allergy and Infectious Diseases, Rockville, Maryland 20852-1742

Received October 20, 2005

Abstract: A rationally designed nucleoside inhibitor of *Mycobacterium tuberculosis* growth (MIC₉₉ = 0.19 μM) that disrupts siderophore biosynthesis was identified. The activity is due to inhibition of the adenylate-forming enzyme MbtA which is involved in biosynthesis of the mycobactins.

Tuberculosis (TB) is the leading bacterial cause of infectious disease mortality. The current WHO-approved treatment for TB, known as directly observed therapy short-course (DOTS), involves a three- or four-drug regimen comprising isoniazid, rifampin, pyrazinamide, and/or ethambutol for a minimum of 6 months.¹ While these first-line agents remain useful in treating susceptible *Mycobacterium tuberculosis* strains, the emergence of multidrug resistant tuberculosis demands the development of new drugs.

Iron acquisition is an indispensable process for many pathogens since this essential nutrient is sequestered by mammalian host proteins such as the transferrins.² Pathogenic microorganisms have evolved a number of mechanisms to overcome this iron restriction, but the most common mechanism involves the synthesis and secretion of low molecular weight, high-affinity iron chelators termed siderophores.³ *M. tuberculosis* produces two series of structurally related peptidic siderophores known as the mycobactins and carboxymycobactins that vary by the appended lipid residue (Figure 1).⁴ Because mycobactins are critical for growth and virulence of *M. tuberculosis*, they have emerged as attractive targets for the development of anti-TB agents.^{5–7}

Elucidation of the biosynthetic pathway of the mycobactins has aided this approach. Biosynthesis begins with an adenylate-forming enzyme, MbtA, which activates and loads salicylic acid onto a mixed nonribosomal peptide synthetase polyketide synthase (NRPS-PKS) assembly line comprised of five other enzymes (MbtB–MbtF) that sequentially build the mycobactin core scaffold (Figure 1).⁸ Additional post NRPS-PKS modifications through lipidation and N-hydroxylations afford the mycobactins (2) and carboxymycobactins (3). MbtA is an ideal target since MbtA has no mammalian homologues. Further, Marahiel and co-workers demonstrated that inhibitors developed for the functionally related aminoacyl tRNA synthetases, which activate amino acids to the corresponding aminoacyl adenylates, can be utilized to inhibit adenylate forming enzymes from NRPS systems despite a lack of either structure or sequence similarity.^{9,10} The cocrystal structure of a homologous adenylating

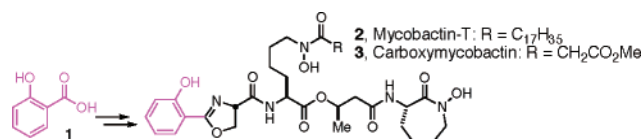


Figure 1. Biosynthesis of the mycobactins and carboxymycobactins. Salicylic acid (1) is converted to mycobactin T (2) and carboxymycobactin (3).⁴ The depicted lipid side chain is a representative as both 2 and 3 are isolated as mixtures with various length lipid residues.

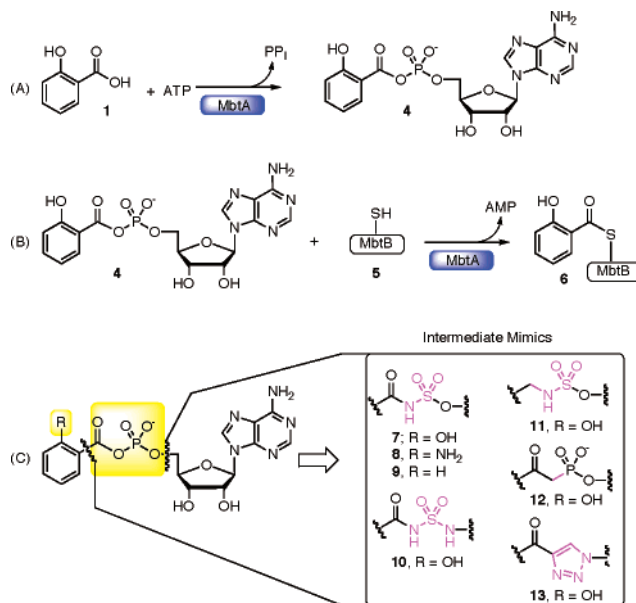


Figure 2. Enzyme reaction mechanism catalyzed by MbtA. (A) First half-reaction. (B) Second half-reaction. (C) Intermediate mimics.

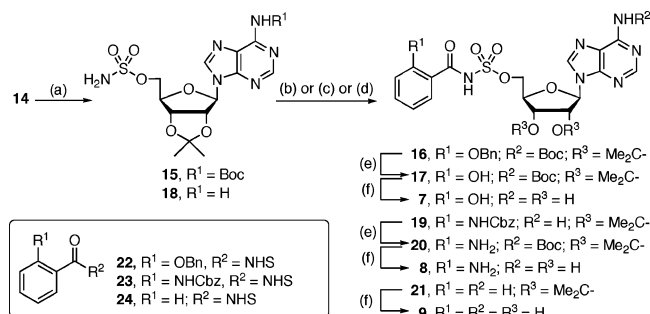
enzyme (DhbE) with its adenylated substrate (2,3-dihydroxybenzoic acid) has been solved, providing both structural and mechanistic insight into the reaction catalyzed by MbtA.¹¹ Last, the catecholate-class of siderophores are characterized by a 2-hydroxyphenyl or 2,3-dihydroxyphenyl moiety at the ‘N-terminus’; consequently, inhibitors toward the adenylation protein MbtA are expected to be useful against the biosynthesis of a wide array of structurally diverse siderophores.³

MbtA incorporates salicylic acid into the mycobactin core scaffold, using a two-step reaction (Figure 2) that is mechanistically similar in all members of the adenylate-forming enzyme superfamily and the functionally related aminoacyl tRNA synthetases.^{12,13} In the first half-reaction, binding of both the substrate acid (1) and ATP is followed by nucleophilic attack of the substrate carboxylate on the α-phosphate of ATP to generate a tightly bound acyl adenylate (4) and the release of pyrophosphate (Figure 2, part A). In the second half-reaction, the enzyme binds the phosphopantetheine (ppan) cofactor (5) of the thiolation domain of MbtB and transfers the acyl adenylate (4) onto the nucleophilic sulfur atom of this cofactor moiety to provide salicyl-bound-MbtB (6) (Figure 2, part B). The rationale for inhibitor development is the tight binding of the acyl adenylate intermediate, which typically binds 3–5 orders of magnitude more tightly than the substrate acid.^{14,15} Therefore, analogues incorporating stable linkers as bioisosteres of the labile acyl phosphate function provide potent enzyme inhibitors. These inhibitors are classified as bisubstrate inhibitors¹⁶ or intermediate mimics¹⁴ and not as mechanism-based inhibitors as recently suggested.¹⁷ The salicyl adenylate scaffold provides

* To whom correspondence should be addressed. Phone: 612-625-7956. Fax: 612-626-5173. E-mail: aldrich015@umn.edu.

[†] University of Minnesota.

[‡] National Institute of Allergy and Infectious Diseases.

Scheme 1^a

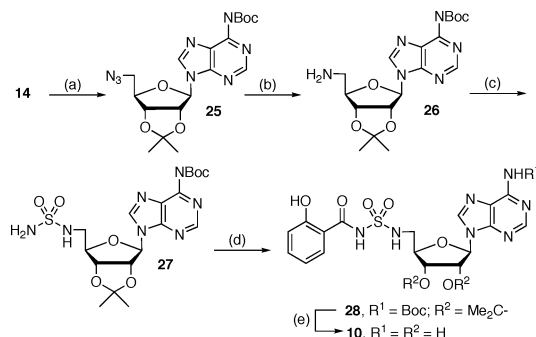
^a Reaction conditions: (a) NH₂SO₂Cl, NaH, 82%; (b) **22**, **15**, Cs₂CO₃: 80% (**16**); (c) **23**, **18**, DBU: 36% (**19**); (d) **24**, **18**, DBU: 44% (**21**); (e) H₂, Pd/C: 95% (**17**); 41% (**20**) (f) 80% aq. TFA: 74% (**7**); 64% (**8**); 100% (**9**).

many opportunities for inhibitor development. In this paper we report our preliminary evaluation of several bioisosteric replacements of the labile acyl phosphate function and investigate the role of the salicyl moiety for activity.

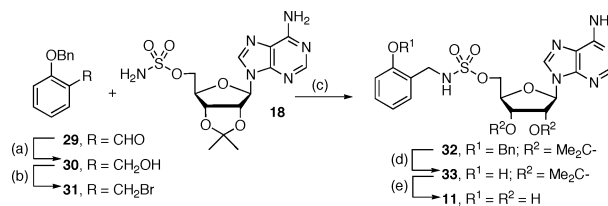
The first inhibitor examined was based on the acylsulfamate linker inspired from the natural product ascamycin, wherein the phosphate moiety is mimicked by the isosteric sulfamate group.¹⁸ The synthesis of **7** began with sulfamoylation of *N*⁶-Boc-2',3'-*O*-isopropylidene adenosine **14**²⁷ to provide sulfamate **15** (Scheme 1). Coupling to the *N*-hydroxysuccinimide (NHS) ester of *o*-benzyl salicylic acid **22** mediated by Cs₂CO₃ afforded **16**.¹⁹ Sequential deprotection of the benzyl ether by catalytic hydrogenation to **17** followed by the isopropylidene acetal and Boc carbamate with aqueous TFA yielded salicyl-sulfamate **7**. An alternative five step synthesis of **7** was recently reported by Ferreras et al.¹⁷ Both anthraniloyl-sulfamate **8** and benzoyl-sulfamate **9** were prepared in an analogous fashion.

The acylsulfamate linkage of inhibitor **7** is extremely acidic with a calculated pK_a of 0.6, while the pK_a of **9** was experimentally determined to be 2.8 (calculated 3.4), demonstrating that the *o*-hydroxy function of the salicyl moiety modulates the acidity of the NH proton through resonance delocalization.²⁰ We have observed that the acylsulfamate linkage is intrinsically unstable as the free acid but considerably more stable as the conjugate base since the negative charge on the nitrogen atom deters nucleophilic attack on the carbonyl function. This is expected to be a principal mechanism of decomposition in analogy to the acylsulfonamides.²¹ Significantly, we found that **8** decomposed rapidly over several days at 25 °C in CD₃OD but was unchanged after 30 days as the triethylammonium salt. Accordingly, all inhibitors were subsequently converted to the triethylammonium salts after purification while conversion to alkali salts is readily achieved through ion-exchange.

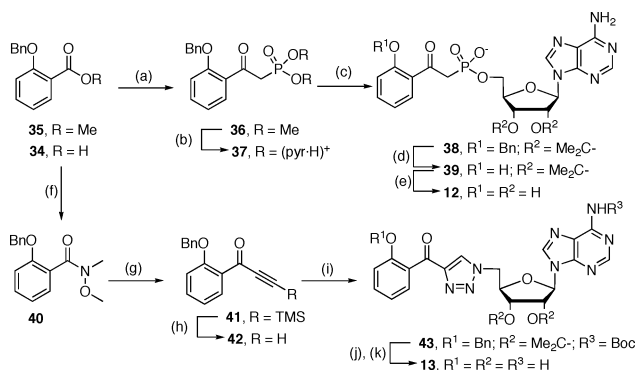
Substitution of the sulfamate oxygen with a nitrogen affords the acylsulfamide linkage of **10** and raises the pK_a of the central NH by approximately 2 units to a calculated value of 2.7. Additionally, the acylsulfamide function was expected to have improved stability relative to the acylsulfamate linkages of **7**–**9**, as 5'-*O*-sulfamoyladenine is preceded to decompose with expulsion of the 5'-*O*-sulfamoyl moiety through both hydrolysis and cyclonucleoside formation.^{22,23} Synthesis of **10** was accomplished by treatment of **14** under Appel conditions to afford the intermediate 5'-bromide that was converted in-situ to the corresponding azide **25** (Scheme 2). Catalytic hydrogenation gave amine **26**, which was sulfamoylated to provide sulfamide **27**. Coupling to salicylic acid mediated by CDI and DBU yielded **28** that was deprotected with aqueous TFA to furnish acylsulfamide **10**.

Scheme 2^a

^a Reaction conditions: (a) CBr₄, PPh₃, NaN₃, 48%; (b) H₂, Pd/C, 70%; (c) NH₂SO₂Cl, NaH, 34%; (d) salicylic acid, CDI, DBU, 40%; (e) 80% aq TFA, 81%.

Scheme 3^a

^a Reaction conditions: (a) NaBH₄, 98%; (b) CBr₄, PPh₃, 88%; (c) Cs₂CO₃, 48%; (d) H₂, Pd/C, 83%; (e) 80% aq TFA, 81%.

Scheme 4^a

^a Reaction conditions: (a) **35**, LiCH₂P(O)(OMe)₂, 88%; (b) (i) TMSBr, (ii) pyr., 100%; (c) TrisylCl, 2',3'-*O*-isopropylidene adenosine, 6%; (d) H₂, Pd/C, 40%; (e) 80% aq TFA, 90%; (f) (i) **34**, (COCl)₂, (ii) Me(OMe)NH₂·HCl, 80%; (g) TMS-acetylene, *n*-BuLi, 76%; (h) TBAF, 79%; (i) **25**, CuSO₄, sodium ascorbate, 89%; (j) H₂, Pd/C; (k) 80% aq TFA, (100%, 2 steps).

To explore the significance of the linkage carbonyl group for activity, analogue **11** was synthesized (Scheme 3). Removal of the carbonyl function also serves to raise the pK_a of the sulfamate NH to a calculated value of 7.5 with an attendant decrease in overall polarity. This was succinctly carried out by NaBH₄ reduction of **29** to provide alcohol **30** that was converted to bromide **31**. Alkylation of 5'-*O*-sulfamoyl adenosine **18** with bromide **31** employing Cs₂CO₃ yielded sulfamate **32** which was deprotected to furnish target inhibitor **11**.

The β-ketophosphonate linkage, which is the closest mimic of the acyl phosphate moiety, was examined next (Scheme 4). Synthesis was initiated by addition of the lithium anion of methyl dimethylphosphonate to methyl benzoate derivative **35** to provide **36**.²⁴ Treatment with TMSBr afforded phosphonic acid **37** that was coupled with 2',3'-*O*-isopropylidene adenosine employing 2,4,6-trimethylbenzenesulfonyl chloride to yield **38**.²⁴ Stepwise deprotection of the benzyl ether to **39** and isopropylidene acetal furnished target inhibitor **12**.

Table 1. Inhibition of *M. tuberculosis* H37Rv^a

inhibitor	MIC ₉₉ (μM)	MIC ₅₀ (μM) ^b
isoniazid	0.18	nd ^c
7	0.29	0.091 ± 0.05
8	>100	30.9 ± 2.5
9	12.5	4.5 ± 1.0
10	0.19	0.077 ± 0.022
11	>100	>100
12	>100	>100
13	>100	>100

^a Grown in GAST Media w/out Fe³⁺; see Supporting Information for details. ^b MIC₅₀ value ± SD (*N* = 4) was obtained from the dose–response curves and corresponds to the drug concentration, which resulted in 50% inhibition of growth. ^c Not determined.

The novel acyltriazole inhibitor **13**, which still maintains the critical four-atom spacer and possesses multiple H-bonding acceptor sites, was the last analogue examined. This was prepared from *O*-benzylsalicylic acid **34** by conversion to Weinreb amide **40** (Scheme 4). Addition of the lithium anion of TMS-acetylene to **40** afforded **41** that was desilylated with TBAF to furnish ynone **42**. The copper(I)-catalyzed Huisgen 1,3-dipolar cycloaddition between ynone **42** and azide **25** provided exclusively the regioisomeric 1,4-disubstituted triazole **43**, which was deprotected to generate the target inhibitor **13**.²⁵

The inhibitors were tested directly against whole-cell *M. tuberculosis* H37Rv under iron-limiting conditions since this allows the concurrent evaluation of binding affinity, stability, and membrane permeability.²⁶ The minimum inhibitory concentrations (MIC) that inhibited >99% of growth are shown in Table 1. The MIC₅₀ values were calculated from the dose–response plots and are also shown in Table 1. Salicyl-sulfamide **10** displayed the highest activity with an MIC₉₉ of 0.19 μM, which rivals the first-line antitubercular isoniazid. Salicyl-sulfamate **7** displayed slightly attenuated activity with an MIC₉₉ of 0.29 μM. The importance of the hydroxy function of the salicyl moiety was examined by deletion using the simple benzoyl analogue **9** which displayed a 66-fold decrease in MIC₉₉, while substitution by an amine in anthraniloyl analogue **8** led to greater than 500-fold loss of activity (MIC₉₉). Inhibitors using either the sulfamate- (**11**), β-ketophosphonate- (**12**), or acyltriazole-linker (**13**) showed no inhibition of growth up to 100 μM.

Recently, the MIC₅₀ of analogue **7** against *M. tuberculosis* H37Rv was reported as 2.2 μM. However, these authors measured the MIC₅₀ value using a much higher cell density (OD₆₂₀ = 0.01 which approximates 10⁷ bacteria/mL) than is typically used, which can lead to underestimation of compound potency due to drug inactivation by the high cell density as well as increased likelihood of resistant mutants.¹⁷

The most potent inhibitors **7** and **10** were evaluated for their ability to inhibit mycobactin biosynthesis utilizing a modified radioassay originally developed by DeVoss and co-workers.^{6,17} *M. tuberculosis* H37Rv (initial OD₆₂₀ = 0.2) was treated with radiolabeled [7-¹⁴C]-salicylic acid and inhibitors or DMSO (0.25%) as a control.²⁷ In the absence of inhibitor, synthesis of both mycobactin and carboxymycobactin was robust while in the presence of either **7** (20 μM) or **10** (10 μM) complete inhibition of mycobactin and carboxymycobactin biosynthesis was observed.

To obtain preliminary data about toxicity for future in vivo studies, the cytotoxicity of inhibitors **7–13** was evaluated against the P388 murine leukemia cell line that has been shown to be sensitive to nucleoside derivatives.²⁷ None of the inhibitors displayed any toxicity up to the maximum concentration tested (ED₅₀ > 100 μg/mL that corresponds to 100–200 μM for **7–13**,

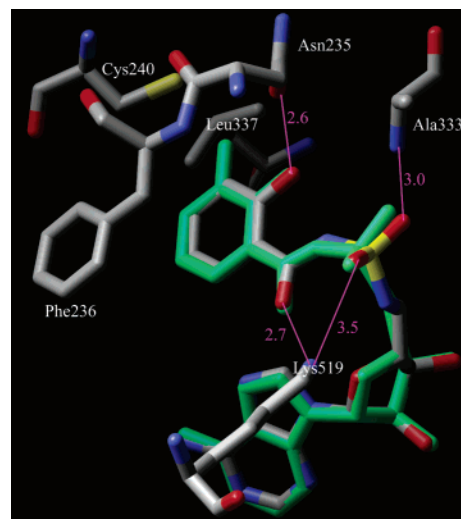


Figure 3. Model of **10** bound to MbtA. Legend: Compound **10** (colored by atom) was modeled into the DhbE active site after making several amino acid changes to reflect the sequence of MbtA. Dihydroxybenzoate from the DhbE X-ray structure is overlaid in green. Key distances in the model of **10** are shown using purple lines with distances in Å. Only key residues affecting salicyl and linker binding are shown. For comparison with the DhbE structure, residues are numbered according to that sequence. Hydrogens removed for clarity.

where ED₅₀ is defined as the concentration of compound that inhibits 50% cell growth), demonstrating the pronounced selectivity of the inhibitors and further validating the inhibitor design strategy. The therapeutic index of the most potent inhibitor **10** (ED₅₀/MIC₅₀) is greater than 900.

Next, the cocrystal structure of DhbE with an adenylated dihydroxybenzoate in the active site was used to construct a model of MbtA and compounds **7–13** were docked into the model.^{11,27} Some activity differences among **7–13** may be due to the geometry of the salicyl/linker region. Dihydroxybenzoate adopts a flat conformation in the DhbE X-ray structure, as do the most active docked compounds, acylsulfamate **7** and acylsulfamide **10**. Both form an internal hydrogen bond between the salicyl *o*-hydroxy and the sulfamate amine. In contrast, quantum calculations show that analogues **8** and **9**, which have lower activity, are inherently unable to adopt the preferred planar conformation because of steric conflicts involving the aryl ortho substituent and the sulfamate amino hydrogen. However, this explanation is only valid if the active site environment changes the pK_a of the nitrogen atom, which is deprotonated in solution. Additional selectivity may arise from interactions of the ortho substituent with Asn235: unlike the more active compounds, **9** lacks the hydroxy necessary to maintain the Asn235 hydrogen bond observed in the DhbE X-ray structure. In the case of **8**, further selectivity could be provided if the Asn235 side chain presents its amino group to the ligand, which would create a preference for hydroxy (**7**) rather than amino (**8**) ortho substituents. However, it is not possible to infer from the DhbE structure which rotamer this side chain adopts in MbtA. Modeling of **11** confirms that reduction of the salicyl carbonyl to a methylene causes the loss of a hydrogen bond to Lys519.

No structural explanation for the inactivity of β-ketophosphonate **12** was observed. The lack of activity is likely a result of hard-ionized phosphate moiety that limits membrane permeability, and this underscores the usefulness of the acylsulfamate and acylsulfamide linkage as phosphate bioisosteres. Although these linkages too are ionized, the charge is highly delocalized. Modeling of triazole **13** showed that hydrogen bonds involving the phosphate of the natural substrate (or sulfamate of **7**) are

lost when a triazole replaces the phosphate. In addition, the planar geometry of the triazole was a poor fit for the binding site, requiring out of plane bending of the ring substituents.

In conclusion, we have designed, synthesized, and evaluated a series of bisubstrate inhibitors of the adenylate-forming enzyme MbtA. These studies focused on the crucial linker domain of the inhibitor scaffold and resulted in the identification of acylsulfamide **10**, which is a potent inhibitor of *M. tuberculosis* growth under iron-limiting conditions. Molecular modeling provided insight into the observed SAR profile, while preliminary studies support the proposed mechanism of action. This strategy represents a promising approach for the development of a new class of antibiotics effective for the treatment of TB.

Acknowledgment. This research was supported by the Center for Drug Design in the Academic Health Center of the University of Minnesota. We thank the Minnesota Supercomputing Institute VWL lab for computer time and Ms. Christine Dreis for performing the cytotoxicity assay.

Supporting Information Available: Experimental details (¹H, ¹³C NMR, HRMS, HPLC) for intermediates and final products, growth inhibition assay of *M. tuberculosis* H37Rv under iron-deficient conditions, dose–response curves for inhibitors **7–10**, cytotoxicity assay, molecular modeling of MbtA, siderophore radioassay, pK_a calculations and measurements. This material is available free of charge via the Internet at <http://pubs.acs.org>.

References

- World Health Organization. *Tuberculosis handbook*; WHO: Geneva, 1998 (WHO/TB/98.253).
- Ratledge, C.; Dover: L. G. Iron metabolism in pathogenic bacteria. *Annu. Rev. Microbiol.* **2000**, *54*, 881–941.
- Crosa, J. H.; Walsh, C. T. Genetics and assembly line enzymology of siderophore biosynthesis in bacteria. *Microbiol. Mol. Biol. Rev.* **2002**, *66*, 223–249.
- Vergne, A. F.; Walz, A. J.; Miller, M. J. Iron chelators from mycobacteria (1954–1999) and potential therapeutic applications. *Nat. Prod. Rep.* **2000**, *17*, 99–116.
- Luo, M.; Fadeev, E. A.; Groves, J. T. Mycobactin-mediated iron acquisition within macrophages. *Nature Chem. Biol.* **2005**, *1*, 149–153.
- De Voss, J. J.; Rutter, K.; Schroeder, B. G.; Su, H.; Zhu, Y.; Barry, C. E. 3rd The salicylate-derived mycobactin siderophores of *Mycobacterium tuberculosis* are essential for growth in macrophages. *Proc. Natl. Acad. Sci. U.S.A.* **2000**, *97*, 1252–1257.
- Wagner, D.; Maser, J.; Lai, B.; Cai, Z.; Barry, C. E. 3rd; zu Bentrup, K. H.; Russell, D. G.; Bermudez, L. E. Elemental analysis of *Mycobacterium avium*-, *Mycobacterium tuberculosis*-, and *Mycobacterium smegmatis*-containing phagosomes indicates pathogen-induced microenvironments within the host cell's endosomal system. *J. Immunol.* **2005**, *174*, 1491–1500.
- Quadri, L. E. N.; Sello, J.; Keating, T. A.; Weinreb, P. H.; Walsh, C. T. Identification of a *Mycobacterium tuberculosis* gene cluster encoding the biosynthetic enzymes for assembly of the virulence-conferring siderophore mycobactin. *Chem. Biol.* **1998**, *5*, 631–645.
- Finking, R.; Neumüller, A.; Solsbacher, J.; Konz, D.; Kretzschmar, G.; Schweitzer, M.; Krumm, T.; Marahiel, M. A. Aminoacyl adenylate substrate analogues for the inhibition of adenylation domains of nonribosomal peptide synthetases. *ChemBiochem* **2003**, *4*, 903–906.
- May, J. M.; Finking, R.; Wiegeshoff, F.; Weber, T. T.; Bandur, N.; Koert, U.; Marahiel, M. A. Inhibition of the D-alanine: D-alanyl carrier protein ligase from *Bacillus subtilis* increases the bacterium's susceptibility to antibiotics that target the cell wall. *FEBS J.* **2005**, *272*, 2993–3003.
- May, J. J.; Kessler, N.; Marahiel, M. A.; Stubbs, M. T. Crystal structure of DhbE, an archetype for aryl acid activating domains of modular nonribosomal peptide synthetases. *Proc. Natl. Acad. Sci. U.S.A.* **2002**, *99*, 12120–12125.
- Gulick, A. M.; Lu, X.; Dunaway-Mariano, D. Crystal structure of 4-chlorobenzoate: CoA ligase/synthetase in the unliganded and aryl substrate-bound states. *Biochemistry* **2004**, *43*, 8670–8679.
- Sieber, S. A.; Marahiel, M. A. Molecular mechanisms underlying nonribosomal peptide synthesis: approaches to new antibiotics. *Chem. Rev.* **2005**, *105*, 715–738.
- Kim, S.; Lee, S. W.; Choi, E.-C.; Choi, S. Y. Aminoacyl-tRNA synthetases and their inhibitors as a novel family of antibiotics. *Appl. Microbiol. Biotechnol.* **2003**, *61*, 278–288.
- Schimmel, P.; Tao, J.; Hill, J. Aminoacyl tRNA synthetases as targets for new anti-infectives. *FASEB J.* **1998**, *12*, 1599–1609.
- Copeland, R. A. In *Evaluation of Enzyme Inhibitors in Drug Discovery*; Wiley: Hoboken, NJ, 2005; pp 202–203.
- Ferreras, J. A.; Ryu, J.-S.; Lello, F. D.; Tan, D. S.; Quadri, L. E. N. Small-molecule inhibition of siderophore biosynthesis in *Mycobacterium tuberculosis* and *Yersenia pestis*. *Nature Chem. Biol.* **2005**, *1*, 29–32.
- Isono, K.; Uramoto, M.; Kusakabe, H.; Miyata, N.; Koyama, H.; Ubukata, M.; Sethi, S. K.; McCloskey, J. A. Ascarycin and dealanylascarycin, nucleoside antibiotics from *Streptomyces* sp.. *J. Antibiot. (Tokyo)* **1984**, *37*, 670–672.
- Castro-Pichel, J.; Garcia-Lopez, M. T.; De las Heras, F. G. A facile synthesis of ascarycin and related analogs. *Tetrahedron* **1987**, *43*, 383–389.
- Klicic, J. J.; Friesner, R. A.; Liu, S.-Y.; Guida, W. C. Accurate prediction of acidity constants in aqueous solution via density functional theory and self-consistent reaction field methods *J. Phys. Chem. A* **2002**, *106*, 1327–1335. Acidity constants were calculated on a truncated model compounds using the pK_a module of Jaguar. See Supporting Information for details.
- Backes, B. J.; Ellman, J. A. Carbon–carbon bond-forming methods on solid support. Utilization of Kenner's 'safety-catch' linker. *J. Am. Chem. Soc.* **1994**, *116*, 11171–11172.
- Shuman, D. A.; Robins, R. K.; Robbins, M. J. The synthesis of adenine 5'-O-sulfamoyl nucleosides related to nucleocidin. *J. Am. Chem. Soc.* **1969**, *91*, 3391–3392.
- Peterson, E. M.; Brownell, J.; Vince, R. Synthesis and biological evaluation of 5'-sulfamoylated purinyl carbocyclic nucleosides. *J. Med. Chem.* **1992**, *35*, 3991–4000.
- Görling, G.; Cramer, F. Synthese von Inhibitoren für die Phenylalanyl-tRNA-Synthetase: Methylen-Analoga des Phenylalanyl-adenylats. *Chem. Ber.* **1973**, *106*, 2460–2467.
- Feldman, A. K.; Colasson, B.; Fokin, V. V. One-pot synthesis of 1,4-disubstituted 1,2,3-triazoles from in situ generated azides. *Org. Lett.* **2004**, *6*, 3897–3899.
- Domenech, P.; Reed, M. B.; Barry, C. E. 3rd Contribution of the *Mycobacterium tuberculosis* MmpL protein family to virulence and drug resistance. *Infect. Immun.* **2005**, *73*, 3492–3501.
- See Supporting information.

JM051060O